

Effect of Zinc Interlayer in Microstructure Evolution and Mechanical Properties in Dissimilar Friction Stir Welding of Aluminum to Titanium

Amlan Kar , Satish V. Kailas, and Satyam Suwas

(Submitted July 11, 2018; in revised form August 28, 2018; published online October 9, 2018)

The welding of aluminum (Al) and titanium (Ti) is difficult and challenging due to the differences in their chemical and physical properties, and the formation of brittle intermetallic phases. In the present experiment, a zinc (Zn) interlayer was used during friction stir welding of Al to Ti. The weld was characterized in detail to understand the mechanisms associated with microstructural evolution and improvement in mechanical properties of the weld. X-ray computed tomography results reveal three-dimensional distribution of particles and flakes of titanium in the weld nugget. It was also observed that Ti particles are inhomogeneously distributed in the weld and the distribution depends on their morphology. Such a distribution of Ti was informative in understanding material flow. In addition, the consolidation of Zn in the Al matrix reveals the nature of material flow in the weld nugget as well. The importance of the Zn interlayer and mechanism of phase formation was explored in this study. It was characterized that the mechanical mixing of Zn with Al and Ti alters phase evolution and restricts the formation of conventional Al_3Ti intermetallic phase. The presence of zinc homogenizes elemental distribution and inhibits the formation of brittle intermetallic phases, which leads to a substantial improvement in mechanical properties of the weld.

Keywords dissimilar friction stir weld, intermetallic phase, mechanical properties, x-ray tomography, zinc interlayer

1. Introduction

Aluminum (Al) and titanium (Ti) have high specific strength and low density, due to which they have high demand in automotive, defense and aerospace industries. Moreover, they possess complimentary thermal and corrosion resistance properties that are in manufacturing hybrid structures. The welding of Al to Ti has attracted attention in making hybrid structures and complex designs wherein a wide range of temperatures is inevitable. In general, conventional fusion welding of Al to Ti is difficult because they possess wide differences in chemical and physical properties, especially the melting point. In addition, the Al/Ti welds suffer from reduced strength and ductility due to the formation of brittle intermetallic phases in the weld nugget because of metallurgical reason and selection of processing parameters (Ref 1, 2). However, the presence of intermetallic phase in any thermo-mechanical processes including conventional welding is inevitable (Ref 3-5). Temperature and exposure time are the two important parameters in the formation of these intermetallics. These limitations promote solid-state welding for joining dissimilar Al and Ti.

Several solid-state welding and controlled fusion welding methods such as diffusion bonding, ultrasonic welding, friction welding, laser welding and pressure welding have been used to join Al with Ti and to mitigate the formation of brittle intermetallic phases. The Al-Ti intermetallics appeared even in diffusion bonded Al-Ti multi-laminated cold-rolled sheets (Ref 6). Later, to improve productivity, laser welding and electron beam welding with shielding gas were used in the Al-Ti system. Creamer et al. (Ref 4) found an intermetallic layer of lesser thickness (2 μm) when joining Al/Ti tailored blanks. It has been illustrated that the growth of intermetallics is almost independent of heat input because of the limited diffusivity of Al in Ti. Fuji (Ref 7) suggested that the formation of intermetallic phases at joint interface is a necessary prerequisite for satisfactory bond formation in dissimilar friction welding.

All the above welding techniques reveal several disadvantages like higher welding temperatures, formation of intermetallic phases in the weld, geometrical and equipment-related limitations along with slow productivity. Hence, an alternative bonding mechanism such as three-dimensional mixing of two materials in the solid-state condition along with temperature-assisted diffusion bonding can be a potential joining mechanism for dissimilar welding. Friction stir welding (FSW) is considered a prospective friction-based solid-state welding process in which heat is generated by friction and leads to the deformation of the workpieces. This process has been used to join Al with Ti. Dressler et al. (Ref 8) demonstrated the feasibility of producing dissimilar butt joints of Ti-6Al-4V and AA2024-T3 by FSW. It was observed that the nugget zone is composed of a mixture of Al matrix and Ti particles. The joint interfaces contained voids in the weld nugget as well. It was proposed that the presence of voids in interface is due to the insufficient flow of titanium particles in aluminum. Chen and Nakata (Ref 9) reported that the maximum failure load of the Al/Ti joint (by FSW) reached 62% of the strength of base Al.

Amlan Kar and Satish V. Kailas, Department of Mechanical Engineering, Indian Institute of Science, Bengaluru 560012, India; Satyam Suwas, Department of Materials Engineering, Indian Institute of Science, Bengaluru 560012, India. Contact e-mail: amlankar@iisc.ac.in.

The formation of intermetallic phases can be restricted by using a third material as an interlayer between Al and Ti during welding (Ref 10). The selection of the interlayer should be such that it promotes the formation of phases that are ductile when compared to brittle Ti-Al intermetallic phases. Fuji et al. (Ref 7, 11) studied friction-welded joints of Ti with super-pure Al, commercially pure (cp) Al and AA5083. It was reported that the as-welded joints had the strength of aluminum, and upon post-weld heat treatment, the tensile strength of the welds deteriorated. This was attributed to the formation of the intermetallic phase Al_3Ti in Ti/pure Al and Ti/cp Al joints along with τ -Al ($Ti_2Mg_3Al_{18}$), Mg_2Al_3 and Al_3Ti in Ti/AA5083 joints. The segregation of silicon acts as a barrier to the formation of Al_3Ti in the case of Ti/cp Al. Therefore, such titanium aluminides have been considered as candidates for high-temperature structural applications. However, their ductility at low temperatures is very low, thereby restricting their application at room temperature.

Some alloying elements, for example zinc (Zn), are expected to induce low-temperature ductility. The Al-Zn phase diagram shows a wide range of solid solubility at different temperatures (Ref 12). It exhibits enhanced diffusivity in a high strain rate process (Ref 13). The reason for the enhanced diffusivity is deformation-induced vacancies and phase stability. Zn and Ti produce a number of intermetallics according to the equilibrium phase diagram (Ref 14). Moreover, the addition of Ti in Zn facilitates grain refinement (Ref 15). The presence of refined and homogeneously distributed intermetallics in a weld nugget can enhance the mechanical properties of the weld by hindering dislocation movements. It can also reduce the direct interaction between Al and Ti; hence, the probability of the formation of the Al_3Ti intermetallic phase decreases with the addition of Zn. In addition, the melting point of zinc is 420 °C, which is considerably lower than that of aluminum (660 °C) and titanium (1670 °C). Therefore, it is expected that Zn will get distributed homogeneously in the weld nugget at the welding temperature and retards the formation of Ti-Al-based intermetallic compounds, leading to the enhancement in mechanical properties of the weld. Therefore, Zn can be used as one of the prospective interlayer materials to enhance the mechanical properties of Al-Ti friction stir welds. In the present experiment, Zn was used as an interlayer in the FSW of Al to Ti. The properties of the weld were systematically characterized to find out the joint formation. The effect of Zn on the microstructural evolution and phase formation was investigated. An attempt was made to explore material flow behavior from volumetric (three-dimensional) distribution of Ti particles and consolidation of Zn in the weld nugget. The mechanical properties of the Al/Ti welds have been investigated in detail to understand the effect of Zn on their final properties.

2. Experimental Procedure

2.1 Materials and Method

Plates of 4-mm-thick commercially pure Al and commercially pure Ti sheet were cleaned using acetone to remove any oxide present in the surface. The 140-mm-long faying surfaces of both the plates were milled to get an even and polished surface. The Al and Ti plates were placed on advancing (AS) and retreating side (RS) of the weld, respectively. A 200- μ m-

thick Zn foils is used as interlayer between Al and Ti as shown in Fig. 1.

Friction stir processing experiment was carried out using a custom-built 3-axis machine in which the tool is kept in a horizontal position and the specimen is held vertical. The machine is developed with the help of IISc Bangalore, India, and ETA Technologies (Pvt.) Ltd., Bangalore, India. The tool used during the experiment was a custom-made cylindrical FSW tool, made of tungsten carbide-cobalt (WC-8% Co), having shoulder and pin diameter of 18 mm and 4 mm, respectively. The length of the tool pin was 3.2 mm, and hence, an effective plunge depth of 3.5 mm was maintained throughout the weld. The tool to workpiece angle (tool tilt angle) was fixed at 2.5°. FSW was performed at tool rotation speed of 900 rpm, welding speed of 90 mm/min and tool offset of 1.6 mm on Al side from faying interface in a single weld. These friction stir weld parameters were obtained using a bottom-up approach of optimization (Ref 16, 17).

2.2 Microstructural Characterization

X-ray micro-computed tomography (XCT) measurements were taken using the Zeiss Versa 520 system. This is a three-dimensional (3D) nondestructive visualization and quantification technique, which can identify each element present within weld nugget. It is equipped with a rotating turntable between the x-ray source and detector. The sample is placed on this rotating table. The x-ray which is focused on the sample was either attenuated or passes through the sample and develops a 2D grayscale radiograph on the screen of the detector. The resolution of the scan is determined by the magnification factor of the object that results from the relative position of the source/detector geometry. A manually selected mode is used to select the number of projections required and auto mode is used to scan through a full 360° rotation, which is then back-projected to reconstruct the 3D volume. Moreover, the sample was placed such that weld zone was positioned within this field of view. The axis of x-ray path and sample transverse cross section were aligned perpendicular to each other. The combined effect of all these parameters yields the resolution of 6 μ m-10 μ m depending on sample dimensions.

To observe the microstructure of the weld, weld plate was sectioned by electro-discharge machining (EDM) perpendicular to the welding direction. The weld samples were polished by the standard metallographic method and subsequently etched

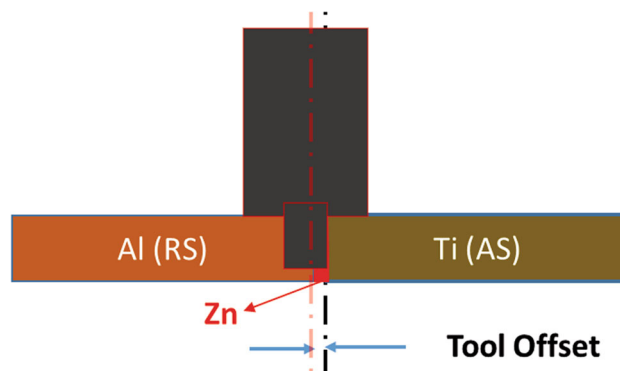


Fig. 1 Schematic image showing the position of Al, Ti and Zn during weld. Zn foil of 200 μ m thickness was placed with Al and Ti plates. Tool interacts with Zn positioned on the AS of the tool

by Kroll's reagent for Ti and Keller's reagent for Al. Optical microscopy of the samples at different tool offset condition was carried out to observe the macrostructure of the weld and shape of the interfaces. The detailed interfacial morphology and chemical composition of the welds were examined by scanning electron microscope (SEM) equipped with an energy-dispersive spectrometer (EDS) and electron probe micro-analyzer (EPMA). To examine the phase evolution in welds, x-ray diffraction (XRD) method was used for all samples using slow step size of 0.033°/step. Samples are placed inside the XRD holder such that the centerline of beam coincides with faying interface of weld.

2.3 Characterization of Mechanical Properties

The mechanical properties of the weld were measured at ambient condition by Vickers micro-hardness and uniaxial tensile testing perpendicular to the weld interface. Vickers hardness was measured across the weld with the load of 200 g and dwell time of 10 s.

Tensile samples were cross-sectioned using EDM perpendicular to the weld direction as per ASTM E8 standard with reduced gauge length of 16 mm. It is to be noted that the diameter of the tool shoulder was 18 mm (less than the gauge length of tensile sample), and hence, the measured tensile property is from the weld zone instead of weld component. Before testing, a thickness of 0.2 mm was removed from bottom and top of the weld to smoothen the surface, and hence, the surface effect had been excluded. Exact dimensions of tensile sample at different regions over the gauge length were measured for each specimen, and the average value was used for calculating the UTS and ductility of the welds. The tensile test of the welds was carried out using a BiSS-UTM instrument at a strain rate of 10^{-3} /s. Fracture surface of the tensile samples was analyzed using SEM.

3. Results

3.1 Distribution of Titanium Particle in the Nugget Zone

A three-dimensional (3D) tomography analysis using XCT shows the presence of Ti in the weld nugget as shown in Fig. 2. To understand the detailed distribution of these fragments, an isometric view is shown along with the top and front views. The isometric view reveals the 3D distribution of fragments,

whereas the top and front view represents the two-dimensional (2D) distribution of Ti fragments from the two directions, respectively. In friction stir welding of aluminum and titanium, Ti fragments (particles and flakes) are distributed in the Al matrix or in the weld nugget due to a shift of the tool axis on the Al side as shown by red symmetric lines in Fig. 2(b).

Stirring of processed materials in FSW depends on the tool position with respect to the faying interface. In most of the dissimilar welding, tool axis is shifted toward Al side or retreating side (RS) of weld from the faying interface (Ref 18-21). The shifting of tool position reduces tool wear, and the possible overheating of lower melting point material is avoided. The tool offset is selected such that it should scribe the harder material, i.e., Ti in dissimilar FSW of Al to Ti, to facilitate mixing and thereby obtaining a sound metallurgical bonding.

Buffa et al. (Ref 22) showed that the bond line and the weld line are not the same in FSW. Non-optimal mixing was observed when the tool position was more than an optimal value (Ref 23, 24). Kumar et al. (Ref 25) as well found out that the amount of mixing was not symmetric in both the longitudinal and transverse direction of the weld line (Ref 21). They further pointed out that plunging the tool into the softer material placed on the retreating side avoids tool wear and breakage (Ref 21). An identical result was obtained by Song et al. (Ref 23) during FSW of 2-mm-thick AA6061 and Ti-6Al-4V with the Ti alloy on the advancing side. It is expected that the optimum tool offset should increase with the choice of two materials having wide differences in physical and mechanical properties; therefore, both the volume of intermixing and homologous temperature could be appropriately balanced. In the present investigation, FSW was performed at a tool offset of 1.6 mm on Al side from the faying interface. Therefore, the red symmetry lines illustrating mixing of Ti particles in Al matrix do not seem to be in the middle in the picture but shift to the Al side of the weld.

The nugget zone displays a composite mixture of Al and Ti fragments. Moreover, these fragments are distributed inhomogeneously in the weld nugget. The agglomeration of fragments in the weld nugget is detrimental leading to the formation of voids due to the discontinuity in material flow (Ref 26). Hence, a detailed investigation on the distribution of these fragments is highly informative.

The fragments are separated by a specific volume range as shown in Fig. 3. It is observed that fine Ti particles (small fragments) are homogeneously distributed in the weld nugget

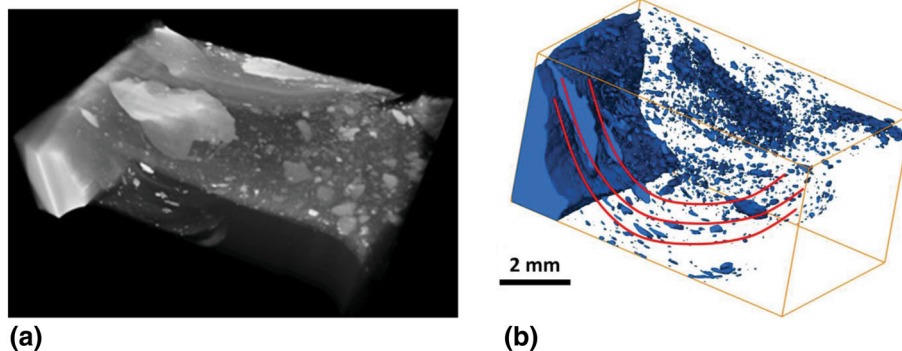


Fig. 2 (a) Isometric view of the weld showing variation in mechanical mixing represented by image contrast, and (b) volumetric distribution of Ti particles in weld nugget indicates inhomogeneous mixing and variation in particle size in the weld

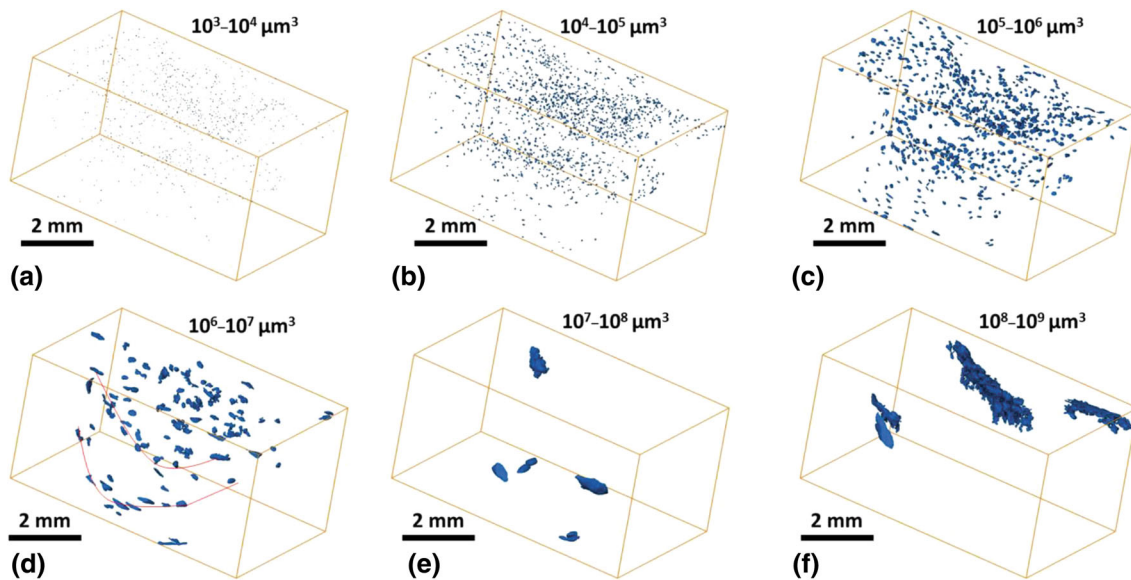


Fig. 3 Isometric view of the weld showing the volumetric distribution of Ti particles in weld nugget based on their volume range as mentioned in each figure. The result indicates that, unlike coarse particles, fine particles are homogeneously distributed in the weld nugget

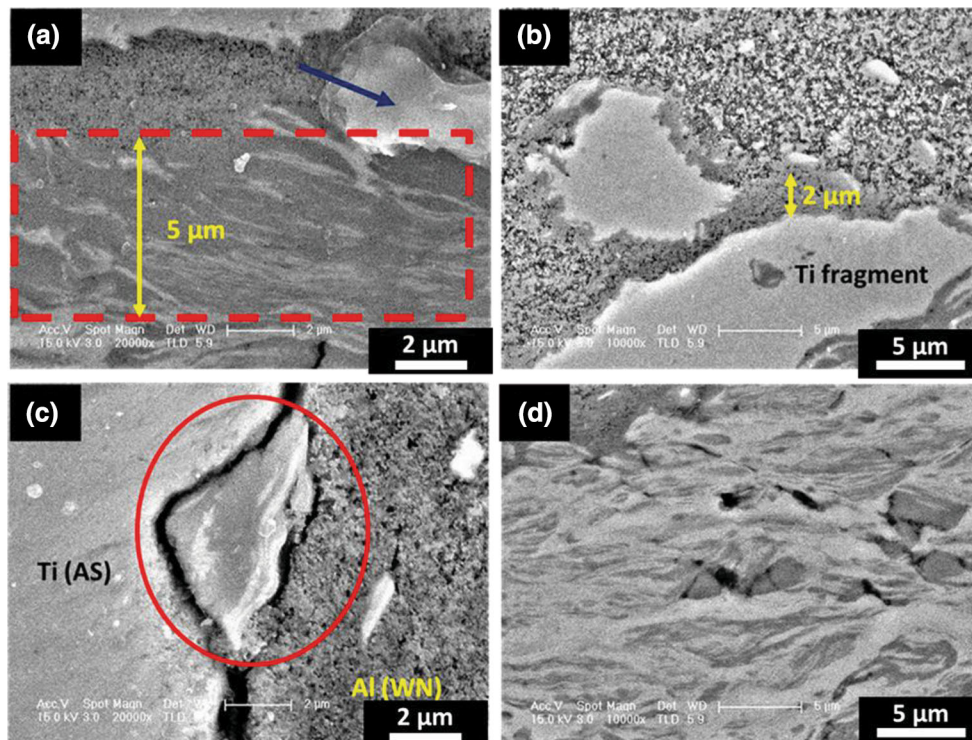


Fig. 4 Scanning electron micrographs from the cross section of the weld with 1.6 mm tool offset showing (a) Al/Ti interface at close to the surface of the weld, (b) Ti particles surrounding diffused interface in nugget zone, (c) Al/Ti joint interface at the nugget zone, (d) intercalated particle in weld nugget

unlike large flakes (large and elongated fragments) of Ti that are consolidated non-uniformly.

3.2 Microstructural Features of the Weld

The cross-sectional SEM micrographs of the Al/Ti interfaces of the joint close to the surface, top side of the faying interface and different types of particles in the weld nugget are shown in

Fig. 4. The contrasting bright and gray colors in the image are Ti and Al, respectively. Zinc is not observed as a separate phase because it primarily forms a solid solution with Al at the welding temperature. From the figure, it can be observed that boundaries of the Ti particles close to the surface are more diffused [5 μm, marked with a red square in Fig. 4(a)] than those of the Ti particles present in the nugget zone [2 μm in

Fig. 4(b)]. The contrast shows a reaction zone between Al and Ti; this reaction has taken place at the interfaces near fine flakes (Fig. 4a). The large Ti particles and flakes present in the same zone do not react with Al at the interfaces [marked with blue arrows in Fig. 4(a)].

In addition, a fine void is observed at the Al/Ti joint interface as shown in Fig. 4(c). At the Ti interface, a particle consisting of Al, Ti and reaction product is also observed (Fig. 4c). The reaction occurs due to severe deformation and temperature rise during the FSW process. The morphology of the interface in the middle of the nugget zone is different compared to the top and the joint interface. Two types of particles and corresponding interfaces are observed as shown in Fig. 4(b) and (d); they are globular Ti particles (Fig. 4a) with limited reaction zone at the interfaces and intercalated particles with severe reaction zone in and around the particles (Fig. 4d). A number of titanium fragments are noticed in the intercalated particles. This indicates that the particles get fragmented and then subjected to reaction, leading to chemical heterogeneity across the particle.

3.3 Phase Formation in the Weld

To examine phase evolution in weld, x-ray diffraction (XRD) patterns were recorded for the weld nugget as shown in Fig. 5. The analyses of the patterns revealed the presence of intermetallic phases (Al_3Ti and TiZn_3) in the weld. TiZn_3 was found to exist in a smaller fraction when compared to Al_3Ti . On the other hand, the Al- and Ti-based intermetallic compound (Al_3Ti) is found in the weld due to mechanical mixing (Ref 27) and thermodynamic reasons (Ref 28, 29).

3.4 Elemental Distribution on an Intercalated Particle

The WDS mapping in Fig. 6 shows the elemental distribution of Al, Ti and Zn in an intercalated particle. Figure 6(a) gives an indication of the presence of Ti in that particle. In Fig. 6(b), orange spots corresponding to the intermetallic Al_3Ti are observed. The self-propagating reaction due to exothermic

heat evolution during the formation of Al_3Ti leads to thermal inhomogeneity within the particles. Therefore, Al_3Ti forms along a line inside the particle due to this self-propagating nature of the reaction adjacent to a Ti rich region, as indicated in Fig. 6(b). A similar feature is observed at the boundary of these particles.

In addition, Zn is observed inside these particles. The atomic concentration of Zn inside the particle is more than that of Al. A Zn-free zone is observed around this particle, which indicates that Ti has higher affinity to Zn. The red spots in Zn mapping (Fig. 6c) correspond to high fraction of Zn that belongs to intermetallic TiZn_3 . The intermetallic phases form inside the particles, and they are distributed within these particles due to the mechanical stirring and thermal inhomogeneity within the particles. It is understood that the mechanical stirring promotes mixing of the elements and subsequent thermal-assisted diffusion leads to the evolution of intermetallic in dissimilar friction stir welding. The evolution of TiZn_3 phase restricts the formation of brittle intermetallic Al_3Ti in the weld.

3.5 Mechanical Property of Weld

3.5.1 Hardness Variation in the Weld. The hardness profile of the weld is shown in Fig. 7. The hardness of the base material was 148 HVN for Ti and 27 HVN for Al. The hardness across the weld cross section reduces from the Ti side to Al side. A large scatter in hardness is observed in the nugget zone, which is attributed to the presence of Ti particles, intermetallic layers and fragments. The hardness is enhanced from the base Al in the nugget zone due to the formation of Al-Zn solid solution and distribution of fine particles. Therefore, it is expected that failure (on tensile testing) would occur on the retreating side of the weld instead of the weld interface.

3.5.2 Tensile Properties of the Optimized Weld. In the present investigation, the tensile test samples were cut from the weld plate, perpendicular to the weld direction with dimension as shown in Fig. 8(a), which is as per ASTM E8 standard with a reduced gauge length of 16 mm. It is to be noted that the diameter of the tool shoulder was 18 mm, and hence, the measured tensile property is from the weld zone. A thickness of 0.2 mm was removed from the bottom and top surface of the weld to smoothen the surface, and hence, the thickness of the specimen is ~ 3.4 mm. The same was used in calculating the tensile properties.

Cross-tensile tests of the as-received Al and the weld were carried out, and the result is shown in Fig. 8(b). Ultimate tensile strength (UTS) and ductility (percent elongation to fracture) of the base Al and the weld were measured from the data obtained from the tensile tests. The maximum UTS and ductility of the as-received Al were 108 MPa and 18%, respectively, whereas the UTS and ductility of the weld were 138 MPa and 48%, respectively. It is seen from the results that the weld exhibits substantially improved tensile properties in terms of UTS and ductility as compared to as-received Al.

The high-magnification image of the fractured surface under SEM reveals details of the deformation and modes of fracture (Fig. 9). It illustrates a bimodal distribution in fracture behavior, namely ductile and brittle modes of fracture (Fig. 9a). In general, intermetallics possess low ductility, and thus, the appearance of brittle fracture is associated with particles and flakes composed of intermetallic phases (Fig. 9b). The ductile fracture appears at non-intermetallic zones such as Al. In addition, the weak Ti interface fails due to interfacial cracks and

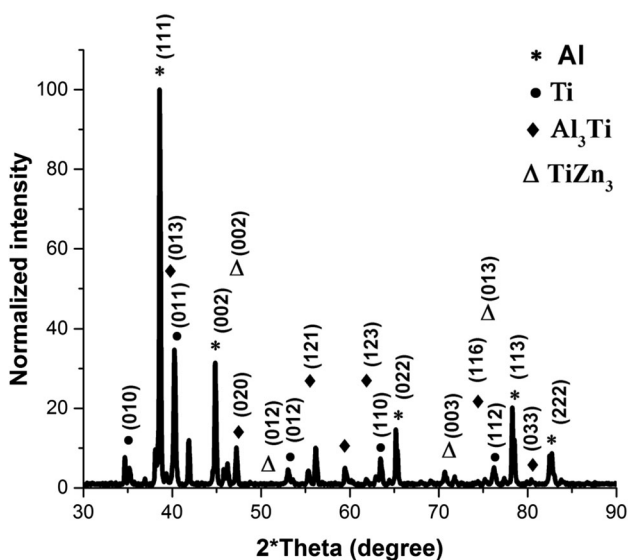


Fig. 5 X-ray diffraction patterns for the samples corresponding to 1.6 mm offset, 900 rpm, 90 mm/min welding speed and 3.5 mm plunge depth showing the evolution of intermetallic phase Al_3Ti and TiZn_3 in the welds

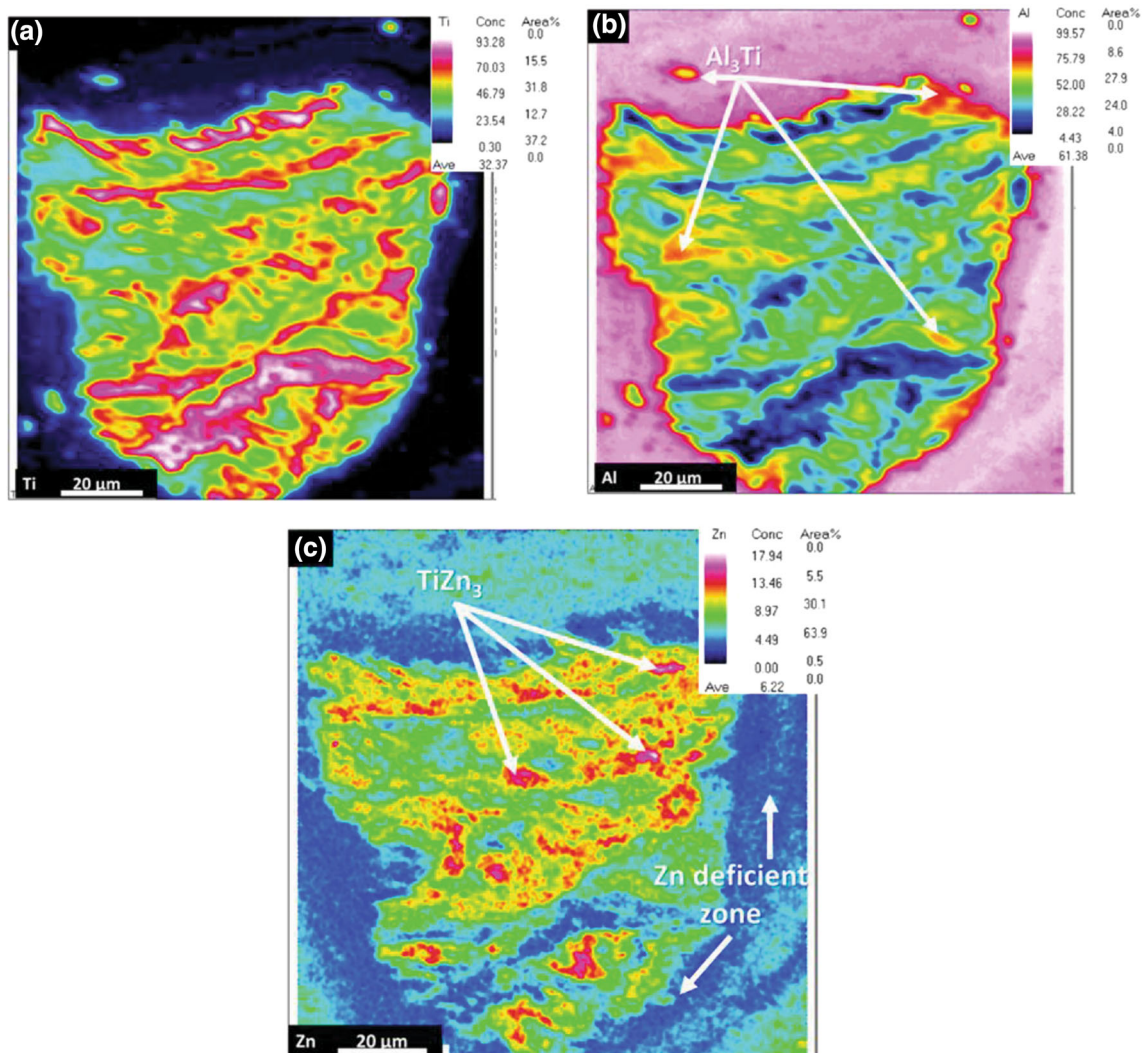


Fig. 6 WDS (EPMA) area dot map of an intercalated particle at the nugget zone corresponding to the optimized tool offset of 1.6 mm exhibiting elemental mixing (at.%) and possible phase evolution within the particle due to mechanical mixing and corresponding thermal diffusion

corresponding crack propagation leading to fracture of the sample. Thus, the final failure across the Ti interface resembles a brittle fracture (Fig. 9b). However, the Al surrounding Ti particles deforms in a ductile mode of fracture as usual. A number of Ti particles are observed at the fracture interfaces, indicating that failure has taken place within the weld nugget. The high-magnification image of ductile fracture reveals that, unlike small dimples, the deep ones are associated with particles. It is also observed that elemental composition of the edge of the dimple is quite different from its interior (Fig. 9c). These zones, along with Ti particles, have evolved due to the addition of Zn in the weld nugget.

4. Discussion

4.1 Mechanical Mixing at the Interfaces and Formation of Intercalated Particles

During the welding process, the tool pin and shoulder encounter both the materials. The tool shoulder is the primary

source of heat generation and deformation because of the higher area of contact, and hence, an enhanced reaction zone and a higher distribution of particles at the top zone of the cross section (Fig. 4a and 10) are witnessed. The semisolid Al with fine Ti particles makes a coating on the surface at the middle and retreating side of the weld where the fraction of Al in the processed volume is more than that of Ti (Fig. 10a). At the advancing side, the thickness of coating reduces and a layer of Ti-Al mixture develops (Fig. 10b). This indicates a transition in mechanical mixing and corresponding variation in deformation and frictional behavior from the retreating to advancing side at the tool shoulder/material interface (Ref 10).

Along the thickness, the tool pin penetrates into the material and generates mechanical stirring. This breaks the Ti in contact with tool at the interface, leading to the formation of particles and flakes and consolidates them in the Al matrix. Therefore, a streamlined mixture composed of Al and Ti is observed at the faying interface (Fig. 10c). The semisolid Al (Al-Zn solid solution) is forced into this fractured zones of Ti because of compressive hydrodynamic stress present in the weld nugget (Fig. 10c) (Ref 30). The local thermal cycle promotes the

reaction between the forged Al-Zn solid solution and the Ti fractured interfaces leading to the formation of intercalated particles and sandwich structure (Ref 10, 31). In addition, the mechanical stirring distributes the particles into Al nugget zone. These particles are, in general, deposited in Al along the flow lines and semisolid Al flows around the pin as per the conventional flow observed in friction stir processing (Ref 32).

Two types of particles and corresponding interfaces are observed as shown in Fig. 4(b) and (d). The globular Ti particles (Fig. 4a) do react with Al uniformly throughout the interface as these particles do not develop fine Ti fragments at the interfaces (Fig. 4a). At these interfaces, local elemental composition and diffusion kinetics are insufficient to initiate the reaction. On the other hand, completely fractured Ti particles are observed in the nugget zone, which get fragmented during the process of deformation as shown in Fig. 4(d). The

fragmentation of Ti particles into fine flakes changes the elemental composition locally and enhances the reaction kinetics due to an increase in the surface-to-volume ratio (Ref 33). In addition, it increases the Al-to-Ti ratio locally, thereby promoting formation of the intermetallic compounds, Al_3Ti . This is the only possible intermetallic compound that evolves in the friction stir welding of Al to Ti (Ref 34). Such intercalation within particles and reaction at interfaces make a strong bond.

4.2 Effect of Zinc on Distribution of Particles

Distribution of particles in the weld nugget can be explained by considering the flow of Ti fragments in the semisolid medium during rotational motion of the tool. In general, these fragments are subjected to drag force. The flakes and large particles with higher and irregular surface area are subjected to higher drag force than fine particles. Therefore, unlike large flakes (Fig. 3d, e and f; volume range $\sim 10^6$ to $10^9 \mu m^3$), fine particles (Fig. 3a, b and c; volume range $\sim 10^3$ to $10^6 \mu m^3$) are carried away with the semisolid Al by mechanical stirring during welding. Hence, these large flakes are non-uniformly consolidated in the weld nugget. The presence of Zn in Al produces a solid solution that reduces the liquidus and solidus temperature of Al in the weld nugget, and hence, flowability of Al in the weld nugget increases further. This enhances the homogeneity in distribution of fine Ti particles (Fig. 3a, b, and c).

4.3 Effect of Zinc on Evolution of Intermetallics

According to the phase diagram, the likely intermetallic phases during welding between Al and Ti are Al_3Ti , $AlTi$ and $AlTi_3$. The evolution of a phase depends on the Gibbs's free energy of that phase at a particular temperature. The brittle intermetallic phase Al_3Ti possesses the lowest Gibbs's free energy of formation in the temperature range 0-1400 °C (Ref 28), and hence, it is expected to evolve during welding. In the present experiment, Al_3Ti is formed at the welding temperature, which is less than 660 °C. In addition, mechanical mixing followed by thermal diffusion leads to the formation of Ti-based intercalated particles (Fig. 4d and 6).

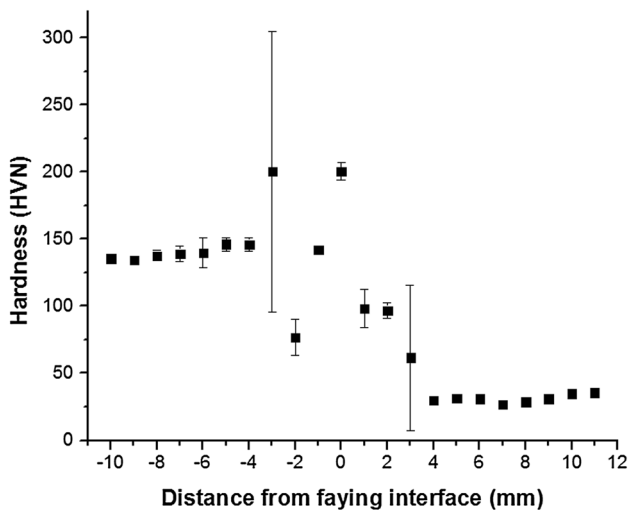


Fig. 7 Hardness variation across the faying interface of the weld with 1.6 mm tool offset. Variation of hardness at WN appears due to the distribution of fragments, intermetallics and partial indentation on these fragments

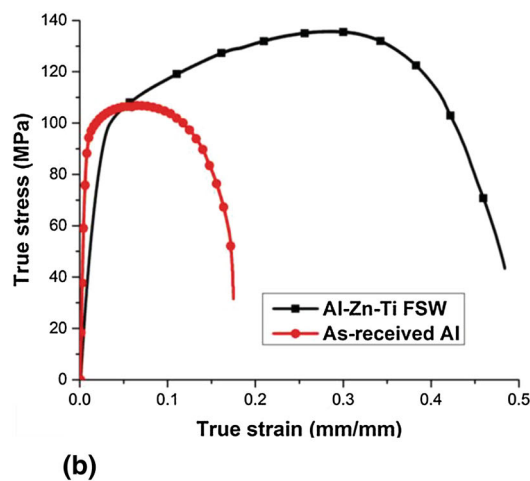
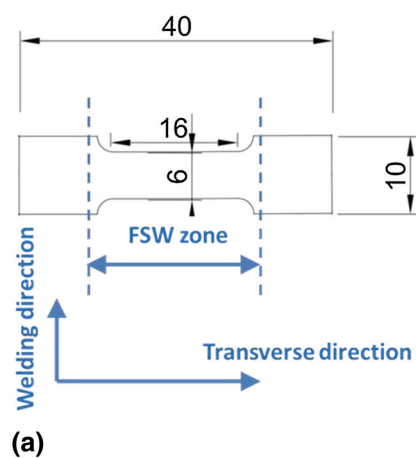


Fig. 8 (a) Geometry and dimension (in mm) of tensile samples including their location with respect to weld geometry, and (b) the stress-strain curve for the weld and the as-received material

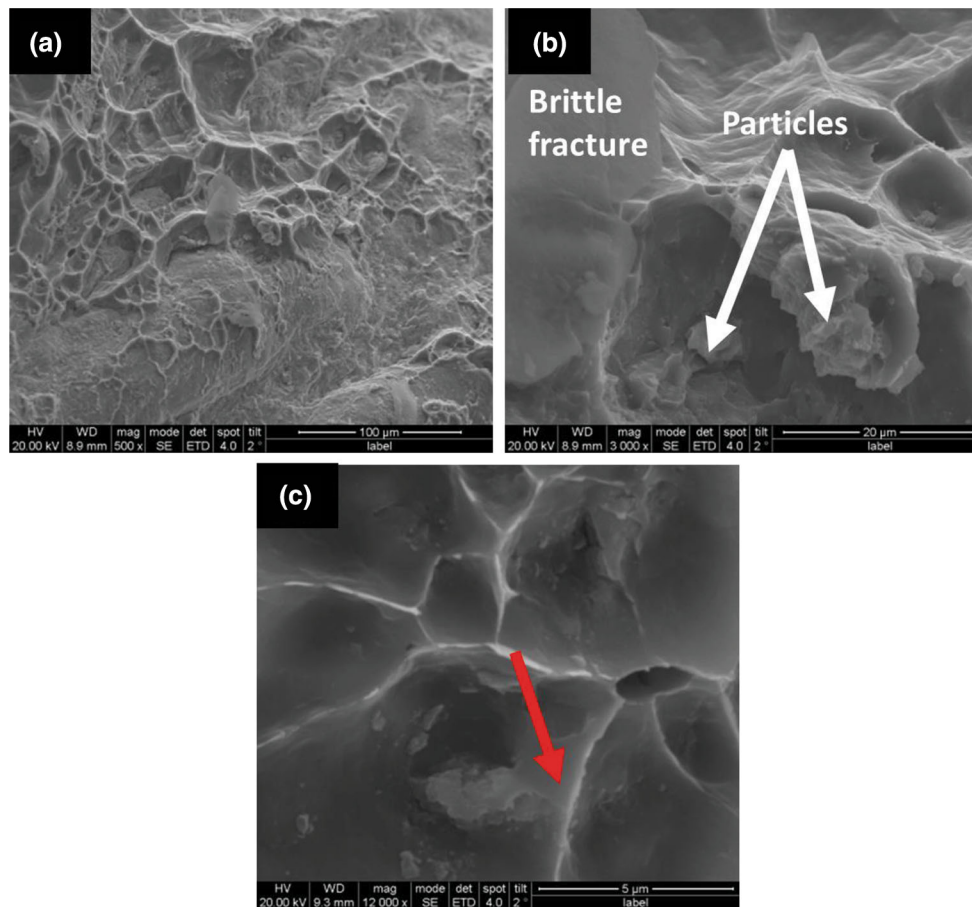


Fig. 9 Fractography of the tensile sample corresponding to 1.6 mm tool offset showing (a) multi-mode fracture; (b) presence of brittle and ductile fracture and (c) presence of Ti fragments on the fracture surface illustrating failure of the sample within weld nugget

The presence of Zn in the weld as an interlayer influences the chemical reaction with both Al and Ti. Zinc is highly soluble in Al at high temperatures: It possesses a high (67 at.%) solubility in Al at 381 °C. The solubility decreases with the decrease in temperature (Ref 35). On the other hand, Zn has a very low solid solubility (less than 0.01 at.%) in Ti (Ref 36). Therefore, Al and Zn form a solid solution without the formation of any intermetallics, whereas Zn reacts with Ti to form a small fraction of intermetallic compound $TiZn_3$ at the welding temperature (Fig. 5). The evolution of $TiZn_3$ is because the reaction between Ti and Zn at a temperature more than the melting point of Zn leads to the formation of Zn rich intermetallics (Ref 37).

The intermetallic phases form inside the particles, and they are distributed within the particles due to mechanical stirring (due to rotation of tool) and thermal inhomogeneity (due to chemical heterogeneity and followed by exothermic reaction) within these particles. It is understood that mechanical stirring promotes the mixing of elements and the subsequent thermally assisted diffusion leads to the evolution of intermetallic compounds in dissimilar FSW. In addition, the evolution of $TiZn_3$ phase in the weld restricts the formation of the brittle intermetallic compound Al_3Ti ; this is because of the formation of Al-Zn solid solution and the consequent low amount of Al that is available to react with Ti. In this context, Delsante et al. (Ref 38) commented that stabilization of Al_3Ti , by substituting

Zn for Al, might offer the possibility of introducing it as a strengthening precipitate in aluminum alloys.

4.4 Effect of Titanium and Zinc on Identifying Material Flow

Figure 2(b) shows the three identical red lines that indicate the alignment of coarse titanium particles. The large flakes and particles obstruct the material flow due to higher surface area-to-volume ratio in the volume range $\sim 10^6$ to $10^7 \mu m^3$ and thereby tend to align along the flow direction to reduce the drag force. Therefore, the alignment of these flakes and particles indicates the material flow, as marked with red lines in Fig. 2(b).

To understand the flow of Al, an elemental mapping of Zn is more useful as the second phase particles gets deposited along the lines of material flow. An EPMA-WDS dot mapping also reveals mixing characteristics in the weld nugget as observed in Fig. 11. A gradient in Zn concentration is observed from the retreating side (RS) to the advancing side (AS). Also, a higher atomic fraction of Zn is observed on the RS and it mixes with Al layer by layer. Zinc is deposited on the RS by centrifugal force along the laminar flow of Al due to rotation of the tool (Ref 39). A similar mixing of Ti in the weld nugget reveals that mechanical mixing in the weld nugget is inhomogeneous and it takes place layer by layer (Fig. 11a). This result illustrates the material flow in the FSW of Al to Ti.

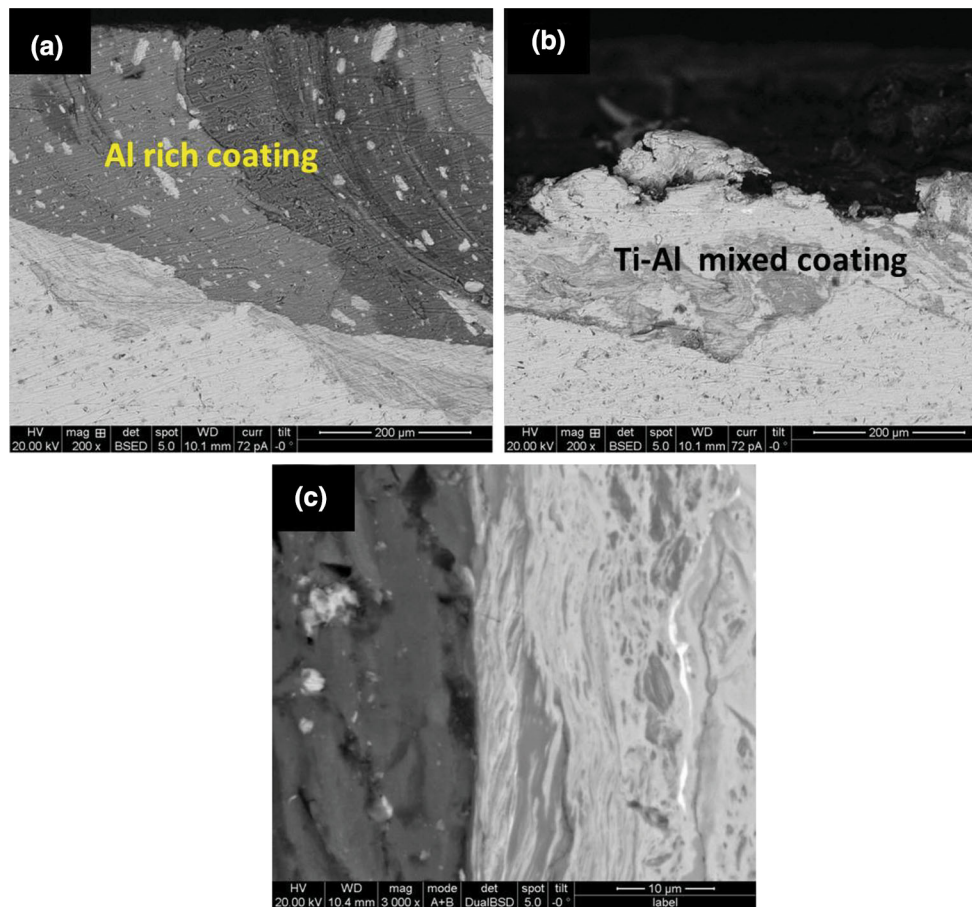


Fig. 10 Backscattered SEM micrographs at Al/Ti interfaces showing (a) Al-based coating on retreating side, (b) Ti-Al coating on advancing side and, (c) swirl-like faying interface at the joint interface corresponding to the optimized tool offset of 1.6 mm

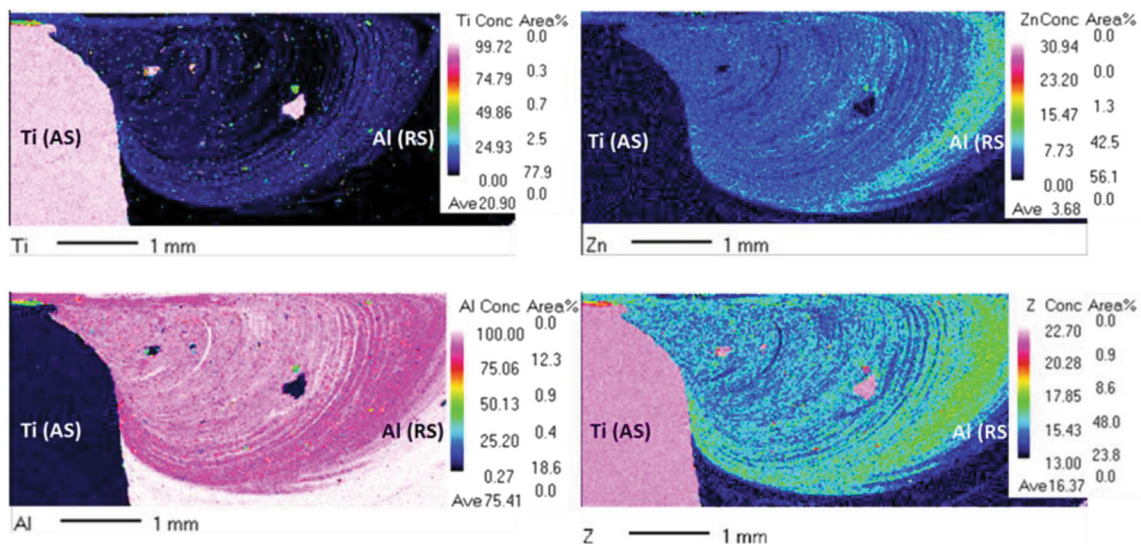


Fig. 11 WDS (EPMA) area dot map of weld cross section corresponding to the optimized tool offset of 1.6 mm exhibiting elemental mixing (in at.%) and its distributions. Layers in material mixing indicate material flow in weld nugget

4.5 Effect of Zinc on Mechanical Properties of the Weld

Since Zn is distributed layer by layer in weld nugget, a gradual reduction in hardness is expected. Moreover, the presence of Ti particles and intermetallic fragments leads to a

fluctuation in hardness of the weld nugget at a certain distance from the joint interface as shown in Fig. 7 (positions: -3 and $+3$). It is interesting to note that no decrease in hardness than that of the base cp Al is noticed in the nugget zone/cp Al

interface due to conventional dissolution of precipitates in the thermo-mechanically affected zone (TMAZ) and heat-affected zone (HAZ). This is due to the fact that the temperature evolution during FSW of Al to Ti with a Zn interlayer is expected to be lower than that in the case of FSW of Al to Ti because of the presence of Zn. It reduces the shear stress, and hence, a lower temperature evolves. The elemental diffusion at a lower temperature not only prevents dissolution of strengthening precipitate but also enhances dislocation density in the weld nugget due to severe deformation, leading to better mechanical properties including superior hardness of the weld nugget.

Hu et al. (Ref 40) reported that the work hardening behavior increased with increasing Zn content in the solid solution, resulting in enhanced uniform elongation. The hardening behavior increases due to the formation of Guinier–Preston (GP) zones, which hinder the movement of dislocations, leading to the formation of slip bands. The presence of slip bands over the gauge length leads to enhanced ductility. Furthermore, dislocations split inside GP zones (Ref 27, 41). Therefore, an extra force is required to move these dislocations leading to an increase in UTS of the weld. Hence, the presence of Zn delays crack propagation resulting in welds with higher ductility along with superior tensile strength.

4.6 Formation of Ti Particles and Its Effect on Mechanical Properties

During friction stir welding of Al/Ti, deformation of Ti occurs at low homologous temperature leading to the formation of adiabatic shear bands (ASB) in Ti. Cracks originate at the edge of ASB during further deformation. Propagation of these crack leads to the formation of Ti particles that are distributed in the weld nugget (Ref 18). During the process, the interface from which the particles have been originated comes in contact with plasticized Al and eliminates the void left behind by the newly developed particle (Fig. 4c). The formation of crack and their elimination, subsequently, is a continuous process. The void and crack observed at the Al/Ti interface are not continuous across the Al/Ti interface. In addition, chemical reaction of Al and Ti at the interface leads to the development of intercalated interface and particles as shown in Fig. 4(c) and (d). Therefore, the discontinuous void and intercalation of Al and Ti at Al/Ti interfaces make the weld stronger.

It is very interesting that the elastic modulus of base Al is higher than that of weld, which can be seen from Fig. 8(b). A number of Ti particles are observed at the fracture interfaces, indicating that failure has taken place within the weld nugget. An EPMA-WDS dot mapping reveals the occurrence of mixing in the weld nugget, as shown in Fig. 11. This confirms that microstructural properties of the weld nugget are different from the as-received Al. Since elastic modulus depends on bonding, atomic distance and crystal structure, the elastic modulus of base Al is different from the weld.

Friction stir welding is a complex deformation process. The complexity in microstructural evolution increases with dissimilar welding, deformation and process parameters. This influences the void size and shape of the porosity which has an effect on the cross-sectional area of the tensile sample. Hence, slope of tensile curve is lower in comparison with a material with lesser amount of void and porosity. The microstructure of the weld exhibits complex mechanical mixing and distribution

of particles. A higher fraction of void and porosity is expected in the weld nugget in comparison with the as-received Al. This could be a contributing factor to the higher measured elastic modulus of base Al than that of the weld.

5. Conclusions

The friction stir welding of cp aluminum to cp titanium with zinc interlayer was been studied in the present investigation. The weld was characterized in detail to understand the mechanisms associated with microstructural evolution, joint formation and mechanical properties. Based on the observations made, the following conclusions can be drawn:

1. The distribution of Ti particles depends on the morphology of particles; fine particles are homogeneously distributed in weld nugget unlike large particles and flakes due to the effect of drag force.
2. The Ti particles and flakes align themselves along the direction of material flow due to high drag force, resembling a trajectory of material flow in the weld nugget. In addition, the development of a solid solution of Zn with Al and the distribution of Zn help in determining the in situ material flow in the weld.
3. The mechanical stirring leads to elemental mixing, and the subsequent thermal cycle promotes the formation of intermetallic compounds. The presence of Zn in Ti-based intercalated particles results in the evolution of a Zn-based intermetallic (TiZn_3), whereas the self-propagating reaction between Al and Ti leads to the formation of a brittle intermetallic compound Al_3Ti due to thermodynamic reasons. The thickness of the intermetallic compound depends on particle size, local elemental composition and temperature evolution in welding.
4. The formation of Al_3Ti is hindered in the presence of Zn. The development of Al-Zn solid solution and Zn-Ti-based phase in and around the intercalated particles restricts the formation of Al_3Ti .
5. The tensile properties of the weld appear superior to that of base Al. The fracture surface exhibits multi-modal fracture behavior including brittle and ductile modes of fracture. The presence of Ti particles on the fracture surface indicates that failure was initiated within the weld nugget and not in the weld interface. The variation in elemental composition within a dimple illustrates that the presence of Zn delays fracture propagation by producing a solid solution with Al, leading to high tensile properties.

Acknowledgments

Authors would like to thank the Defense Research and Development Organization (DRDO), Department of Science and Technology (DST), Ministry of Human Resources Development (MHRD), India, for support and research funding. We would also like to thank Institute X-ray Facility and Advanced Facility for Microscopy and Microanalysis (AFMM) at Indian Institute of Science (IISc), Bangalore, for providing the facilities.

References

1. T. Saeid, A. Abdollah-zadeh, and B. Sazgari, Weldability and Mechanical Properties of Dissimilar Aluminum–Copper Lap Joints Made by Friction Stir Welding, *J. Alloys Compd.*, 2010, **490**, p 652–655
2. Z. Liu, S. Ji, and X. Meng, Improving Joint Formation and Tensile Properties of Dissimilar Friction Stir Welding of Aluminum and Magnesium Alloys by Solving the Pin Adhesion Problem, *J. Mater. Eng. Perform.*, 2018, **27**, p 1404–1413
3. R. Borrisutthekul, Y. Miyashita, and Y. Mutoh, Dissimilar Material Laser Welding Between Magnesium Alloy AZ31B and Aluminum Alloy A5052-O, *Sci. Technol. Adv. Mater.*, 2005, **6**, p 199–204
4. H.-B. Chen, K. Yan, T. Lin, S.-B. Chen, C.-Y. Jiang, and Y. Zhao, The Investigation of Typical Welding Defects for 5456 Aluminum Alloy Friction Stir Welds, *Mater. Sci. Eng. A*, 2006, **433**, p 64–69
5. P. Liu, Y. Li, H. Geng, and J. Wang, Microstructure Characteristics in TiG Welded Joint of Mg/Al Dissimilar Materials, *Mater. Lett.*, 2007, **61**, p 1288–1291
6. S.-Y. Kim, S.-B. Jung, C.-C. Shur, Y.-M. Yeon, and D.-U. Kim, Mechanical Properties of Copper to Titanium Joined by Friction Welding, *J. Mater. Sci.*, 2003, **38**, p 1281–1287
7. M.K.A. Fuji, T.H. North, K. Ameyama, and M. Aki, Mechanical Properties of Titanium-5083 Aluminum Alloy Friction Joints, *Mater. Sci. Technol.*, 1997, **13**, p 673–678
8. U. Dressler, G. Biallas, and U. Alfaro Mercado, Friction Stir Welding of Titanium Alloy TiAl6V4 to Aluminium Alloy AA2024-T3, *Mater. Sci. Eng. A*, 2009, **526**, p 113–117
9. Y.C. Chen and K. Nakata, Microstructural Characterization and Mechanical Properties in Friction Stir Welding of Aluminum and Titanium Dissimilar Alloys, *Mater. Des.*, 2009, **30**, p 469–474
10. Q. Zheng, X. Feng, Y. Shen, G. Huang, and P. Zhao, Dissimilar Friction Stir Welding of 6061 Al to 316 Stainless Steel Using Zn as a Filler Metal, *J. Alloys Compd.*, 2016, **686**, p 693–701
11. A. Fuji, K. Ameyama, and T.H. North, Influence of Silicon in Aluminium on the Mechanical Properties of Titanium/Aluminium Friction Joints, *J. Mater. Sci.*, 1995, **30**, p 5185–5191
12. D. Yang, P. Hodgson, and C. Wen, The Kinetics of Two-Stage Formation of TiAl₃ in Multilayered Ti/Al Foils Prepared by Accumulative Roll Bonding, *Intermetallics*, 2009, **17**, p 727–732
13. I. Gunduz, T. Ando, E. Shattuck, P. Wong, and C. Doumanidis, Enhanced Diffusion and Phase Transformations During Ultrasonic Welding of Zinc and Aluminum, *Scr. Mater.*, 2005, **52**, p 939–943
14. V. Maier, H.W. Höppel, and M. Göken, Nanomechanical Behaviour of Al-Ti Layered Composites Produced by Accumulative Roll Bonding, *J. Phys. Conf. Ser.*, 2010, **240**, p 012108
15. G. Çam, G. İpekoğlu, and H. Tank Serindağ, Effects of Use of Higher Strength Interlayer and External Cooling on Properties of Friction Stir Welded AA6061-T6 Joints, *Sci. Technol. Weld. Join.*, 2014, **19**, p 715–720
16. K.S. Anil Kumar, S.M. Murigendrappa, and H. Kumar, A Bottom-Up Optimization Approach for Friction Stir Welding Parameters of Dissimilar AA2024-T351 and AA7075-T651 Alloys, *J. Mater. Eng. Perform.*, 2017, **26**, p 3347–3367
17. N. Nadammal, S.V. Kailas, and S. Suwas, A Bottom-Up Approach for Optimization of Friction Stir Processing Parameters: A Study on Aluminium 2024-T3 alloy, *Mater. Des.*, 2015, **65**, p 127–138
18. A. Kar, S. Suwas, and S.V. Kailas, Two-Pass Friction Stir Welding of Aluminum Alloy to Titanium Alloy: A Simultaneous Improvement in Mechanical Properties, *Mater. Sci. Eng. A*, 2018, **733**, p 199–210
19. K.-S. Bang, K.-J. Lee, H.-S. Bang, and H.-S. Bang, Interfacial Microstructure and Mechanical Properties of Dissimilar Friction Stir Welds between 6061-T6 Aluminum and Ti-6%Al-4%V Alloys, *Mater. Trans.*, 2011, **52**, p 974–978
20. H. Uzun, C. Dalle Donne, A. Argagnotto, T. Ghidini, and C. Gambaro, Friction Stir Welding of Dissimilar Al 6013-T4 To X5CrNi18-10 Stainless Steel, *Mater. Des.*, 2005, **26**, p 41–46
21. A. Wu, Z. Song, K. Nakata, J. Liao, and L. Zhou, Interface and Properties of the Friction Stir Welded Joints of Titanium Alloy Ti6Al4V with Aluminum Alloy 6061, *Mater. Des.*, 2015, **71**, p 85–92
22. G. Buffa, L. Donati, L. Fratini, and L. Tomesani, Solid State Bonding in Extrusion and FSW: Process Mechanics and Analogies, *J. Mater. Process. Technol.*, 2006, **177**, p 344–347
23. Z. Song, K. Nakata, A. Wu, J. Liao, and L. Zhou, Influence of Probe Offset Distance on Interfacial Microstructure and Mechanical Properties of Friction Stir Butt Welded Joint of Ti6Al4V and A6061 Dissimilar Alloys, *Mater. Des.*, 2014, **57**, p 269–278
24. P. Cavaliere, F. Panella, Effect of Tool Position on the Fatigue Properties of Dissimilar 2024-7075 Sheets Joined by Friction Stir Welding, *J. Mater. Process. Technol.*, 2008, **206**, p 249–255
25. K.S. Kumar, Positional Dependence of Material Flow in Friction Stir Welding: Analysis of Joint Line Remnant and Its Relevance to Dissimilar Metal Welding, *Sci. Technol. Weld. Join.*, 2010, **15**, p 305–311
26. M. Pourali, A. Abdollah-zadeh, T. Saeid, and F. Kargar, Influence of Welding Parameters on Intermetallic Compounds Formation in Dissimilar Steel/Aluminum Friction Stir Welds, *J. Alloys Compd.*, 2017, **715**, p 1–8
27. Q. Zhang, B.L. Xiao, and Z.Y. Ma, Mechanically Activated Effect of Friction Stir Processing in Al-Ti Reaction, *Mater. Chem. Phys.*, 2013, **139**, p 596–602
28. M. Sujata, S. Bhargava, and S. Sangal, On the Formation of TiAl₃ During Reaction Between Solid Ti and Liquid Al, *J. Mater. Sci. Lett.*, 1997, **16**, p 1175–1178
29. M. Sujata, S. Bhargava, S. Suwas, and S. Sangal, On Kinetics of TiAl₃ Formation During Reaction Synthesis from Solid Ti and Liquid Al, *J. Mater. Sci. Lett.*, 2001, **20**, p 2207–2209
30. K. Kumar and S.V. Kailas, On the Role of Axial Load and the Effect of Interface Position on the Tensile Strength of a Friction Stir Welded Aluminium Alloy, *Mater. Des.*, 2008, **29**, p 791–797
31. A. Abdollah-Zadeh, T. Saeid, and B. Sazgari, Microstructural and Mechanical Properties of Friction Stir Welded Aluminum/Copper Lap Joints, *J. Alloys Compd.*, 2008, **460**, p 535–538
32. T.U. Seidel and A.P. Reynolds, Two-Dimensional Friction Stir Welding Process Model Based on Fluid Mechanics, *Sci. Technol. Weld. Join.*, 2003, **8**, p 175–183
33. A. Fuji, In Situ Observation of Interlayer Growth During Heat Treatment of Friction Weld Joint Between Pure Titanium and Pure Aluminium, *Sci. Technol. Weld. Join.*, 2002, **7**, p 413–416
34. Y. Wei, J. Li, J. Xiong, F. Huang, F. Zhang, and S.H. Raza, Joining Aluminum to Titanium Alloy by Friction Stir Lap Welding with Cutting Pin, *Mater. Charact.*, 2012, **71**, p 1–5
35. M. Kreimeyer, F. Wagner, and F. Vollertsen, Laser Processing of Aluminum–Titanium-Tailored Blanks, *Opt. Lasers Eng.*, 2005, **43**, p 1021–1035
36. J.L. Murray, The Ti-Zn (Titanium–Zinc) System, *Bull. Alloy Phase Diagr.*, 1984, **5**, p 52–56
37. W.-S. Lee and C.-F. Lin, Plastic Deformation and Fracture Behaviour of Ti-6Al-4V Alloy Loaded with High Strain Rate Under Various Temperatures, *Mater. Sci. Eng. A*, 1998, **241**, p 48–59
38. A. Kar, S. Suwas, and S.V. Kailas, *An Investigation on Friction Stir Welding of Aluminum to Titanium Using a Nickel Interlayer*, Indian Institute of Welding-International Congress, 2017
39. E. Sharghi and A. Farzadi, Simulation of Strain Rate, Material Flow, and Nugget Shape During Dissimilar Friction Stir Welding of AA6061 Aluminum Alloy and Al-Mg2Si Composite, *J. Alloys Compd.*, 2018, **748**, p 953–960
40. X. Sauvage, G. Wilde, S.V. Divinski, Z. Horita, and R.Z. Valiev, Grain Boundaries in Ultrafine Grained Materials Processed by Severe Plastic Deformation and Related Phenomena, *Mater. Sci. Eng. A*, 2012, **540**, p 1–12
41. V.I. Nizhenko, Free Surface Energy as a Criterion for the Sequence of Intermetallic Layer Formation in Reaction Couples, *Powder Metall. Met. Ceram.*, 2004, **43**, p 273–279